ISBN: 978-3-95450-261-5 ISSN: 2673-7000 doi: 10.18429/JACoW-NAPAC2025-THP028

DIGITAL TWIN FRAMEWORK FOR PIP-II LINAC: AI-DRIVEN MULTI-SCALE MODELING FROM ION SOURCE TO 800 MeV

A. Pathak*, P. Hanlet, T. Miceli
Fermi National Accelerator Laboratory, Batavia, IL, USA

Abstract

The PIP-II linac will enable more than 1.2 MW beam power for DUNE, requiring unprecedented operational reliability across its warm front end (RFQ, MEBT) and five distinct SRF sections operating at 162.5/325/650 MHz. We present a comprehensive digital-twin framework that combines a fully differentiable fast beam-transport core with neural-network surrogates trained on high-fidelity PIC simulations, capturing space charge and nonlinear dynamics beyond traditional envelope codes while achieving $10^4\times$ speedup at $< 1\%$ accuracy. End-to-end differentiability enables gradient-based optimization across 500+ parameters simultaneously (impractical with previous tools), while the model incorporates static/dynamic errors and serves as a virtual-commissioning platform for diverse hardware integration. The framework facilitates reinforcement learning for pulsed/CW mode transitions, predictive maintenance through anomaly detection, and autonomous tuning algorithm development with real-time execution capability. Validation against physics simulations shows excellent agreement for the front end, with initial results indicating potential for 30% commissioning-time reduction and proactive fault mitigation, providing a scalable blueprint for operating next-generation high-intensity accelerators.

INTRODUCTION

The PIP-II SRF linac will deliver more than 1.2 MW beam power for DUNE, with a chopped front end (RFQ, MEBT) feeding five SRF sections at 162.5/325/650 MHz. High-current operation imposes tight uncontrolled-loss limits (order 1 W/m in low-energy sections) and frequent retuning under microphonics, detuning, thermal drifts, and hardware constraints [1–3].

Conventional online toolchains—fast linear/second-moment transport with occasional PIC checks—are mismatched to these requirements: envelope models miss nonlinear space-charge and field-map effects that drive halo and loss, while PIC is generally too slow for shot-to-shot supervisory use or many-parameter optimization. Recent advances in differentiable beam-physics [4], controls-integrated virtual accelerators [5, 6], and data-driven optimization/anomaly detection [7–9] enable a different approach.

We present a controls-integrated, *end-to-end differentiable* digital twin for the PIP-II front end. A symplectic transport core M is augmented by a learned surrogate K_θ trained on high-fidelity PIC to capture nonlinear space charge and RF effects, with measured disturbances injected via $E(\xi)$. The mapping, objectives, and gradients are used for state estimation, virtual diagnostics, and (when enabled) tuning under EPICS with policy safeguards. **Scope:** this paper reports read-only (shadow/replay) validation on RFQ→MEBT and HWR lattices, demonstrating task-level accuracy within target tolerances at $\sim 10^4\times$ runtime speedup; closed-loop operation is summarized briefly.

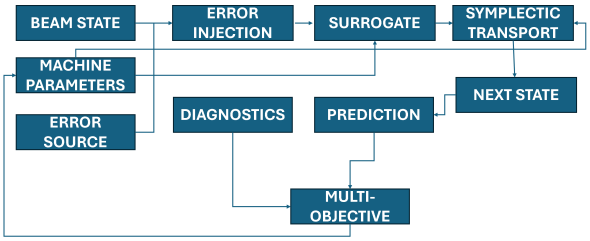

Figure 1: Overview of the differentiable mapping $x_{k+1} = M(p_k) \circ K_\theta(x_k, p_k) \circ E(\xi_k)$ and the objective $J(\mathbf{p})$ that compares predictions $\hat{\mathbf{y}}(s;\mathbf{p})$ to measurements $\mathbf{y}_{\text{obs}}(s)$.

DIGITAL TWIN FRAMEWORK

Problem Formulation

Let $\mathbf{p} \in \mathbb{R}^{N_P}$ denote machine parameters (RF amplitudes/phases, magnet gradients, correctors, chopper timing) and $\mathbf{x}$ the beam state. The differentiable state update is

$$\mathbf{x}_{k+1} = \Phi_\theta(\mathbf{x}_k, \mathbf{p}_k, \xi_k) = M(\mathbf{p}_k) \circ K_\theta(\mathbf{x}_k, \mathbf{p}_k) \circ E(\xi_k), \quad (1)$$

where M is a symplectic transport core, K_θ a learned surrogate trained on PIC data, and E injects error processes ξ_k (misalignments, phase/voltage jitter, microphonics, ripple).

For tuning, we minimize a loss comparing predictions to measurements and penalizing longitudinal mismatch and loss proxies:

$$\min_{\mathbf{p}} J(\mathbf{p}) = \sum_{s\in\mathcal{S}} \Big[w_{\text{orb}} \|\mathbf{y}_{\text{obs}}(s) - \hat{\mathbf{y}}(s;\mathbf{p})\|_2^2 + w_{\text{long}}\, \mathcal{L}_{\text{long}}(s) + w_{\text{loss}}\, \mathcal{R}_{\text{loss}}(s) \Big], \quad (2)$$

where $\mathcal{S}$ indexes BPM/TOF/toroid locations, $\hat{\mathbf{y}}$ are virtual diagnostics from the twin, $\mathbf{y}_{\text{obs}}$ are measurements, $\mathcal{L}_{\text{long}}$ penalizes phase/energy errors, and $\mathcal{R}_{\text{loss}}$ penalizes loss proxies (e.g., halo mass beyond $n\sigma$). Robust variants evaluate J under sampled ξ (expectation or CVaR_α) without optimizing over ξ. Figure 1 summarizes the mapping in Eqs. (1)–(2) and the associated objective.

* abhishek@fnal.gov. This manuscript has been authored by Fermi Forward Discovery Group under Contract No. 89243024CSC000002 with the U.S. Department of Energy, Office of Science, Office of High Energy Physics.

ISBN: 978-3-95450-261-5 ISSN: 2673-7000 doi: 10.18429/JACoW-NAPAC2025-THP028

Learned Physics Operator

The surrogate K_θ applies a differentiable kick that captures collective and RF nonlinearities omitted by M:

$$\Delta\boldsymbol{\pi}_i = f_\theta(\mathbf{r}_i, \mathbf{p}, \mathbf{c}), \qquad \Delta\mathbf{r}_i = g_\theta(\mathbf{r}_i, \mathbf{p}, \mathbf{c}), \tag{3}$$

where $(\mathbf{r}_i, \boldsymbol{\pi}_i)$ are particle coordinates and momenta, $\mathbf{c}$ encodes local optics/field descriptors, and $\mathbf{p}$ are machine settings *(not momenta)*. Training minimizes

$$\mathcal{L}(\theta) = \lambda_1 \sum_t \|\hat{\mathbf{x}}_t - \mathbf{x}_t^{\mathrm{PIC}}\|_2^2 + \lambda_2\, \mathcal{L}_{\mathrm{moments}} + \lambda_3\, \mathcal{L}_{\mathrm{stability}}\,, \tag{4}$$

with trajectory/moment errors and stability regularization.

ARCHITECTURE AND IMPLEMENTATION

The digital twin comprises four cooperating layers: a differentiable physics core that realizes the state update in Eqs. (1) and (2); a data and training pipeline that supplies high-fidelity targets; an orchestration layer for objectives, constraints, and optimizers; and a controls layer that binds the twin to EPICS with a safety policy.

Physics Layer

The beam state advances via $M(\mathbf{p}_k) \circ K_\theta(\mathbf{x}_k, \mathbf{p}_k) \circ E(\xi_k)$ as in Eq. (1). The symplectic transport $M(\mathbf{p})$ uses elementwise maps for drifts, magnets, and SRF cavities parameterized by fields/gradients/phases; energy gain and longitudinal phase advance are applied within M to maintain section-to-section consistency. The learned surrogate K_θ applies a differentiable kick that corrects M for nonlinear space-charge and RF field-map effects by acting on particle coordinates $(\mathbf{r}_i, \boldsymbol{\pi}_i)$ and local descriptors $\mathbf{c}$ to produce $\Delta\mathbf{r}_i, \Delta\boldsymbol{\pi}_i$ (Eq. 3); the composition preserves end-to-end differentiability of $\mathbf{x}_{k+1}$ with respect to $\mathbf{p}$.

The error operator $E(\xi)$ injects measured or synthesized disturbances ξ (misalignments, amplitude/phase jitter, microphonics, ripple); robust evaluations of $J(\mathbf{p})$ use expectation or CVaR_α over sampled ξ, while gradients are taken only with respect to $\mathbf{p}$. Virtual diagnostics $\hat{\mathbf{y}}(s; \mathbf{p})$ are generated by applying measurement models (BPM response, TOF projections, current transformers/toroids) to the propagated state, enabling like-for-like comparisons to $\mathbf{y}_{\mathrm{obs}}(s)$ in Eq. (2).

Data and Training Layer

High-fidelity targets for K_θ are produced with PIC using 3D field maps across domain-randomized operating points (phase/voltage scans, optics settings, controlled mismatch). Training minimizes Eq. (4) with trajectory/state error, moment consistency, and stability regularization; inputs/outputs are normalized, and cross-validation is performed on hold-out lattices and scans. In this work, surrogates are trained offline; during replay, light-weight online calibration (e.g., gains/biases) may be applied based on residual analysis.

Orchestration Layer

The objective $J(\mathbf{p})$ (Eq. 2) aggregates orbit/phase/energy tracking with loss-aware penalties (e.g., halo mass beyond $n\sigma$). Constraints include actuator bounds, slew-rate limits, feasibility projection, and machine-protection guards (MPS) represented as convex boxes with simple nonconvex checks. Projected gradient methods (L-BFGS/Adam) use auto-diff through M+K_θ+E; risk is evaluated as expectation or CVaR_α over sampled ξ. For this contribution, optimizers run in shadow/replay to produce sensitivity analyses and to rank corrective actions; actuator writes are disabled.

Controls Layer (EPICS Binding)

The twin exposes PV maps for synchronized read subscriptions and, when enabled, safe writes mediated by a policy (bounds, rate limits, MPS guard rails, rollback). A translation layer maps PVs to model parameters $\mathbf{p}$ and to measurement operators for $\hat{\mathbf{y}}(s; \mathbf{p})$ so the objective compares like-for-like signals. All interactions are audit-logged with configuration hashes for M, the K_θ checkpoint, and the objective.

Determinism and Reproducibility

Shadow/replay executions are deterministic given a configuration: samplers for ξ are seeded, surrogate checkpoints are fixed, and optics are versioned. Data products record software versions, surrogate IDs, dataset hashes, PV snapshots, and seeds; figure scripts regenerate plots directly from these logged artifacts.

MODES OF OPERATION AND USE CASES

The twin is designed to operate in four modes spanning commissioning and routine operations; this work uses read-only modes (see Fig. 2). (i) *Monitoring (digital shadow)*: read-only mirror that performs state estimation and what-if prediction from live diagnostics, producing virtual diagnostics $\hat{\mathbf{y}}(s; \mathbf{p})$ for comparison with $\mathbf{y}_{\mathrm{obs}}(s)$ in $J(\mathbf{p})$; (ii) *Replay / passive learning*: time-synchronized replays of BPM/TOF/FFC/toroid/LLRF streams for optics/phasing inference, residual analysis, anomaly ranking, and calibration refinement; (iii) *Controller (hybrid closed loop)*: supervisory optimization using $\nabla_{\mathbf{p}} J$ from Eqs. (1)–(2) with feasibility projection, issuing rate-limited EPICS writes under MPS guard rails and automatic rollback; (iv) *Online learning (adaptive closed loop)*: controller mode with in-situ surrogate/calibration updates driven by residuals and replay batches under the same safety policy. *Scope in this paper: (i)–(ii) only; (iii)–(iv) planned.*

Use cases. *Pulse→CW transitions*: multi-parameter ramps (RF phases/voltages, chopper duty) optimized subject to bounds/rate limits/MPS, validated in shadow/replay before live execution; *Autonomous tuning*: multi-objective fits to orbit/envelope/TOF with loss proxies (e.g., halo mass beyond $n\sigma$) in $J(\mathbf{p})$; corrective actions ranked in shadow mode with actuator-aware feasibility projection; *Predictive maintenance*: unsupervised detectors (parity-space/autoencoders)

ISBN: 978-3-95450-261-5 ISSN: 2673-7000 doi: 10.18429/JACoW-NAPAC2025-THP028

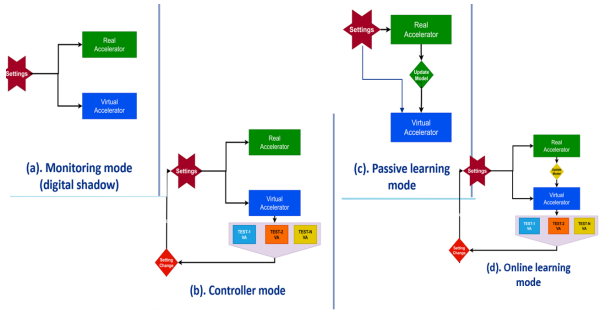

Figure 2: Modes of operation: (a) Monitoring (digital shadow), (b) Replay / passive learning, (c) Controller (hybrid closed loop), (d) Online learning (adaptive closed loop). Results here concern (a)–(b); (c)–(d) are planned.

on LLRF/interlock streams gate controller updates and trigger replay-based diagnosis; *HLA pretesting*: ORM, analyzer, and orbit-correction HLAs exercise the same APIs for reproducible transition from virtual to live operation.

CONTROL SYSTEM INTEGRATION

We operated the twin in *read-only* mode with a direct EPICS binding via a soft IOC. Subscriptions covered BPM, TOF/FFC, toroid, and LLRF PVs (amplitude, phase, detune, interlocks). A translation layer mapped PVs to model parameters $\mathbf{p}$ and to measurement operators to produce virtual diagnostics $\hat{\mathbf{y}}(s;\mathbf{p})$ for like-for-like comparisons in $J(\mathbf{p})$. Data were assembled into time-synchronized frames with timestamps and configuration hashes of M, the K_θ checkpoint, and $E(\xi)$ settings.

Each frame traversed a deterministic pipeline: state estimation (optics/phasing reconstruction), residual analysis, and objective/sensitivity evaluation via auto-diff through $M+K_\theta+E$. The twin then created *ranked* candidate corrections as actuator deltas (RF phases/voltages, magnet gradients, chopper timing) with predicted impact on orbit/phase/energy and loss proxies; actuator writes remained disabled and suggestions were exported for operator review. Feasibility constraints used online (actuator bounds, slew-rate limits, RF family couplings) were enforced during ranking; MPS/interlock PVs gated suggestions, and all candidates underwent policy "dry-run" checks even in read-only mode.

Reproducibility was ensured by logging PV snapshots, software versions, dataset hashes, surrogate IDs, and random seeds for ξ, enabling exact replay of shadow/replay runs. The same EPICS-facing API was exercised by existing HLAs (ORM, analyzer, orbit correction) to verify compatibility and rehearse commissioning workflows without issuing writes.

VALIDATION AND INITIAL RESULTS

Validation targeted the RFQ→MEBT interface and HWR cells using two datasets: (i) PIC-derived holdouts with domain-randomized phases/voltages and controlled mismatch, and (ii) time-synchronized measurement replays (BPMs, TOF/FFC, toroids, LLRF). The twin ran in read-only mode; virtual diagnostics $\hat{\mathbf{y}}(s;\mathbf{p})$ were compared to measurements $\mathbf{y}_{\text{obs}}(s)$ inside $J(\mathbf{p})$.

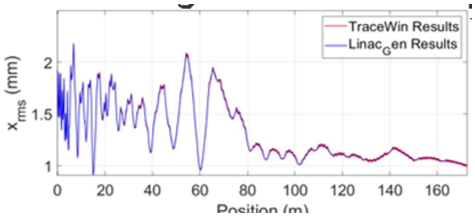

Figure 3: Representative rms envelope comparison: $x_{\text{rms}}(s)$ from PIC versus the twin.

Accuracy was assessed on state/moment trajectories $(x_{\text{rms}}(s), y_{\text{rms}}(s))$, longitudinal projections (ϕ, W), transmission, and a halo indicator (mass beyond $n\sigma$). Across phase and voltage scans and controlled mismatch, envelopes and longitudinal projections matched within target tolerances; transmission and halo proxies remained consistent with PIC references. Replay runs reproduced optics/phasing and reduced residuals on BPM/TOF streams in a manner consistent with the inferred corrections. Runtime was benchmarked as mean wall-clock per meter of lattice propagation for identical lattice/diagnostic sampling. Figure 3 shows a representative envelope comparison used for this assessment. The differentiable core with the learned kick delivered the expected $\sim 10^4\times$ speedup versus high-fidelity references at task-level accuracy suitable for shadow/replay decision support.

DEVELOPMENT PHASES AND REPRODUCIBILITY

Development proceeded in five tightly scoped phases: (i) data & specification—operating envelopes, diagnostics, and error models were defined and PIC campaigns generated; (ii) modeling—M was built and K_θ designed (element-wise for magnets/cavities or block-wise per cell), with uncertainty channels $E(\xi)$ instrumented; (iii) training and validation—domain randomization with hold-out lattices/scans, cross-validation against PIC and measurement replays, and calibration procedures; (iv) controls binding—PVs were mapped to $\mathbf{p}$ and measurement operators, shadow mode implemented, and cycle-time determinism verified; (v) closed-loop trials—candidate policies exercised in safe mode under MPS constraints, with promotion of proven recipes to operations.

Reproducibility is ensured via configuration hashes for optics/objectives, surrogate checkpoints for K_θ, fixed seeds for ξ, and PV snapshots; all artifacts (software versions, datasets) are versioned, and the figure scripts regenerate plots identically from logged runs.

OUTLOOK

Ongoing work extends surrogate coverage to the full SRF chain, tightens uncertainty quantification, and generalizes controllers to multi-beam user modes. The same architecture supports hardware-in-the-loop tests and portable deployment across machines with similar front-end topologies.

ISBN: 978-3-95450-261-5 ISSN: 2673-7000 doi: 10.18429/JACoW-NAPAC2025-THP028

REFERENCES

[1] M. A. Plum, "Beam loss in linacs," in *Beam Loss and Accelerator Protection*, CERN Yellow Reports: School Proceedings, CERN-2016-002, pp. 39–62, 2016. doi:10.5170/CERN-2016-002.39

[2] L. Tchelidze and J. Stovall, "Beam loss limits in high power proton linear accelerators," in *Proc. IPAC'13*, Shanghai, China, 2013, pp. 3930–3932.

[3] R. Stanek *et al.*, "PIP-II project overview and status," in *Proc. SRF'23*, Grand Rapids, MI, USA, 2023, pp. 19–24. doi:10.18429/JACoW-SRF2023-MOIXA02

[4] J. Kaiser *et al.*, "Bridging the gap between machine learning and particle accelerator physics with high speed, differentiable simulations," *Phys. Rev. Accel. Beams*, vol. 27, p. 054601, 2024. doi:10.1103/PhysRevAccelBeams.27.054601

[5] P. Zhu *et al.*, "Multi user virtual accelerator at HEPS for high level application development and beam commissioning," in *Proc. ICALEPCS'23*, Cape Town, South Africa, 2023, pp. 1388–1390. doi:10.18429/JACoW-ICALEPCS2023-THPDP033

[6] S. A. Mnisi, "Systems modeling, AI/ML algorithms applied to control systems," in *Proc. ICALEPCS'23*, Cape Town, South Africa, 2023, pp. 257–261. doi:10.18429/JACoW-ICALEPCS2023-TU1BCO03

[7] R. Roussel *et al.*, "Bayesian optimization algorithms for accelerator physics," *Phys. Rev. Accel. Beams*, vol. 27, p. 084801, 2024. doi:10.1103/PhysRevAccelBeams.27.084801

[8] A. Eichler, J. Branlard, and J. H. K. Timm, "Anomaly detection at the European XFEL using a parity space based method," *Phys. Rev. Accel. Beams*, vol. 26, p. 012801, 2023. doi:10.1103/PhysRevAccelBeams.26.012801

[9] M. M. Rahman *et al.*, "Accelerating cavity fault prediction using deep learning at Jefferson Laboratory," *Mach. Learn.: Sci. Technol.*, vol. 5, no. 3, p. 035078, 2024. doi:10.1088/2632-2153/ad7ad6